Two novel loci underlie natural differences in *Caenorhabditis elegans* macrocyclic lactone responses

Kathryn S. Evans[1,2], Janneke Wit[1], Lewis Stevens[1,a], Steffen R. Hahnel[1], Briana Rodriguez[1], Grace Park[1], Mostafa Zamanian[1,b], Shannon C. Brady[1,2], Ellen Chao[1], Katherine Introcaso[1], Robyn E. Tanny[1], and Erik C. Andersen[1,*]

[1]Molecular Biosciences, Northwestern University, Evanston, IL

[2]Interdisciplinary Biological Sciences Program, Northwestern University, Evanston, IL

[a]Present address: Tree of Life, Wellcome Sanger Institute, Cambridge CB10 1SA, UK

[b]Present address: Department of Pathobiological Sciences, School of Veterinary Medicine, University of Wisconsin, Madison, Wisconsin 53705

***Corresponding author:**

E-mail: erik.andersen@northwestern.edu (ECA)

Abstract

Parasitic nematodes cause a massive worldwide burden on human health along with a loss of livestock and agriculture productivity. Anthelmintics have been widely successful in treating parasitic nematodes. However, resistance is increasing, and little is known about the molecular and genetic causes of resistance. The free-living roundworm *Caenorhabditis elegans* provides a tractable model to identify genes that underlie resistance. Unlike parasitic nematodes, *C. elegans* is easy to maintain in the laboratory, has a complete and well annotated genome, and has many genetic tools. Using a combination of wild isolates and a panel of recombinant inbred lines constructed from crosses of two genetically and phenotypically divergent strains, we identified three genomic regions on chromosome V that underlie natural differences in response to the macrocyclic lactone (ML) abamectin. One locus was identified previously and encodes an alpha subunit of a glutamate-gated chloride channel (*glc-1*). Here, we validate and narrow two novel loci using near-isogenic lines. Additionally, we generate a list of prioritized candidate genes identified in *C. elegans* and in the parasite *Haemonchus contortus* by comparison of ML resistance loci. These genes could represent previously unidentified resistance genes shared across nematode species and should be evaluated in the future. Our work highlights the advantages of using *C. elegans* as a model to better understand ML resistance in parasitic nematodes.

Author Summary

Parasitic nematodes infect plants, animals, and humans, causing major health and economic burdens worldwide. Parasitic nematode infections are generally treated efficiently with a class of drugs named anthelmintics. However, resistance to many of these anthelmintic drugs, including macrocyclic lactones (MLs), is rampant and increasing. Therefore, it is essential that we understand how these drugs act against parasitic nematodes and, conversely, how nematodes gain resistance in order to better treat these infections in the future. Here, we used the non-parasitic nematode *Caenorhabditis elegans* as a model organism to study ML resistance. We leveraged natural genetic variation between strains of *C. elegans* with differential responses to abamectin to identify three genomic regions on chromosome V, each containing one or more genes that contribute to ML resistance. Two of these loci have not been previously discovered and likely represent novel resistance mechanisms. We also compared the genes in these two novel loci to the genes found within genomic regions linked to ML resistance in the parasite *Haemonchus contortus* and found several cases of overlap between the two species. Overall, this study highlights the advantages of using *C. elegans* to understand anthelmintic resistance in parasitic nematodes.

Introduction

Parasitic nematodes pose a significant health and economic threat, especially in the developing world [1–3]. These infections increase morbidity and exacerbate the deleterious effects of malaria, HIV, and tuberculosis [4]. Morbidity varies in severity but commonly affects people in tropical and subtropical regions. It is estimated that over one billion people are infected by one or more species of parasitic roundworm [5], and the loss of disability-adjusted life years caused by these parasites ranks among the top of all Neglected Tropical Diseases [1]. In addition to their devastating impacts on human health, several parasitic nematode species infect a variety of crops and livestock. These infections cause severe economic burdens worldwide [6].

Parasitic nematodes are primarily treated using a limited number of anthelmintic drugs from one of the three major drug classes: benzimidazoles, nicotinic acetylcholine receptor agonists, and macrocyclic lactones (MLs). However, the efficacies of these anthelmintics can be limited by the ubiquitous resistance observed in veterinary parasites [7] and the emerging resistance in human parasites [8,9]. In many cases, resistance is highly heritable, suggesting the evolution of anthelmintic-resistant nematodes might occur under drug selection [10]. We must understand the drug mode of action and identify the genetic loci that contribute to resistance in parasitic nematodes to provide effective long-term treatments. Abamectin and ivermectin are two common MLs used to treat parasitic nematodes of agricultural, veterinary, or human importance [11]. However, widespread resistance to MLs has been reported and is a significant concern [10]. Genetic screens and selections performed in the laboratory-adapted reference strain of the free-living nematode *Caenorhabditis elegans* have identified three genes that encode glutamate-

gated chloride (GluCl) channel subunits (*glc-1*, *avr-14*, and *avr-15*) and are targeted by MLs in *C. elegans* [12,13]. In contrast to *C. elegans* laboratory experiments, several resistant parasitic nematode isolates have been discovered that do not have mutations in genes that encode GluCl subunits [14,15], suggesting that alternative mechanisms of resistance to MLs must exist. Recently, quantitative trait loci (QTL) mappings in both free-living and parasitic nematode species have identified several genomic regions of interest containing genetic variation that confers drug resistance [14,16–20].

The identification of specific genes or variants involved in the molecular basis of drug resistance in parasitic nematodes can be challenging for several reasons. First, their life-cycles require hosts and are costly to maintain [21]. Second, most species do not have annotated genomes assembled into full chromosomes. To date, the most complete genome is *Haemonchus contortus*, which enables genetic mappings and comparative genomic approaches [14,22]. Finally, most species lack key molecular and genetic tools such as CRISPR-Cas9 genome editing [23]. By contrast, the free-living nematode *C. elegans* has a short life cycle that is easy to grow in the laboratory, a well annotated reference genome, and a plethora of molecular and genetic tools to characterize anthelmintic responses [19,20,24–26]. Genetic mappings using hundreds of genetically and phenotypically diverged wild strains of *C. elegans* collected around the world could identify novel loci that contribute to anthelmintic resistance across natural populations [20,24].

Here, we use genome-wide association and linkage mapping analyses to identify three large-effect QTL on chromosome V that contribute to abamectin resistance. One of these QTL was previously identified and is known to be caused by variation in the GluCl

97 channel gene *glc-1* [24,26]. The remaining two QTL are novel. We used near-isogenic
98 lines (NILs) to validate and narrow each QTL independently and identified promising
99 candidate genes to test using CRISPR-Cas9 genome editing. We searched for
100 orthologous genes within ivermectin-response QTL on chromosome V of *H. contortus* and
101 discovered 40 genes present in QTL for both species. This study demonstrates the value
102 of natural variation in the *C. elegans* population to identify candidate genes for resistance
103 and enables understanding of the molecular mechanisms of anthelmintic resistance.
104

105 ## Results

106 **Two different quantitative genetic mapping techniques reveal loci that underlie**
107 **differential responses to abamectin**

108 Anthelmintic resistance can be described as a function of nematode development
109 and reproduction. To quantify *C. elegans* drug resistance, we previously developed a
110 high-throughput assay that uses a flow-based device to measure the development and
111 reproduction of thousands of animals across hundreds of independent strains (see
112 Methods) [19,20,27–33]. In this assay, nematode development is described by a
113 combination of animal length, animal optical density (body thickness and composition
114 integrated by length), and normalized animal optical density (body thickness and
115 composition normalized by length). Although length and optical density are often highly
116 correlated, these three traits can each describe a unique aspect of development [31]. In
117 addition to development, this assay describes nematode reproduction by an
118 approximation of animal brood size. Using this assay, we exposed four genetically
119 divergent strains (N2, CB4856, JU775, and DL238) to increasing doses of abamectin (**S1**

File). In the presence of abamectin, nematodes were generally smaller, less optically dense, and produced smaller broods compared to non-treated nematodes, suggesting an abamectin-induced developmental delay and decreased reproduction (**S1 Fig**). We also observed significant phenotypic variation among strains in response to abamectin, indicating that genetic variation might underlie differences in the abamectin response across the *C. elegans* species.

To investigate the genetic basis of natural abamectin resistance, we exposed 210 wild isolates to abamectin and measured their developmental rates and brood sizes (**S2 File**). These data were used to perform genome-wide association mappings that identified a total of six QTL across the four traits on chromosomes II, III, and V (**S2 Fig, S3 File**). The most significant QTL was detected for brood size on the right arm of chromosome V (VR) and was also detected for animal length (**Fig 1A**). Notably, this region (**Table 1**) includes a gene (*glc-1*) that encodes a subunit of a glutamate-gated chloride (GluCl) channel, which has been previously discovered to underlie phenotypic differences in both swimming paralysis [24] and survival [26] in the presence of abamectin. Additionally, a second QTL on the left arm of chromosome V (VL) underlies differences in both animal length and optical density (**Fig 1A, S2 Fig, S3 File**). This secondary region (**Table 1**) has not been identified in previous *C. elegans* QTL mapping studies [24,26] and thus can be considered a novel region underlying abamectin response.

Table 1. Genomic regions on chromosome V significantly correlated with abamectin resistance.

QTL	Association mapping[1]	Linkage mapping[2]	NIL-defined interval
VL	V:1,757,246-4,333,001	V:2,629,324-3,076,312	V:1-3,120,167
VC	NA	V:6,118,360-7,342,129	V:5,260,997-5,906,132
VR (*glc-1*)[3]	V:15,983,112-16,599,066	V:15,933,659-16,336,743	13,678,801-19,303,558

[1]Mean animal length
[2]Mean animal optical density
[3]From previous data [24]

In parallel to the genome-wide association mapping, we measured animal development and reproduction in abamectin for a panel of 225 recombinant inbred advanced intercross lines (RIAILs) generated by a cross between the N2 and CB4856 strains [31] (**S4 File**). Linkage mapping analysis for all four traits identified a total of 14 QTL on chromosomes II, V, and X including three distinct QTL on chromosome V (**Fig 1B, S3 Fig, S5 File**). Two of the three QTL on chromosome V (VL and VR) overlap with the intervals identified using association mapping (**Fig 1C, Table 1, S4 Fig, S7 File**), suggesting that a single variant both present in the CB4856 strain and prevalent within the natural population might cause the differences in abamectin responses observed in both mapping populations. In fact, a four-amino-acid deletion in the gene *glc-1* that has been previously correlated with abamectin resistance is known to segregate not only among the *C. elegans* population but also between the N2 and CB4856 strains [24,26]. By contrast, the third locus on the center of chromosome V (VC) was only detected using linkage mapping, which suggests that a rare variant in the CB4856 strain underlies this QTL. Regardless, all three loci on chromosome V can be investigated further by leveraging the genetic variation between the N2 and CB4856 strains. At each of the three loci on chromosome V, RIAILs with the CB4856 allele were correlated with abamectin

166 resistance (longer and denser animals) compared to RIAILs with the N2 allele (**S3 Fig,**
167 **S4 and S5 Files**). To search for evidence of any genetic interactions between loci, we
168 performed a two-dimensional genome scan. We found no significant interactions on
169 chromosome V or otherwise (**S5 Fig, S6 File**), suggesting that each of the three loci
170 additively contribute to abamectin resistance.

171

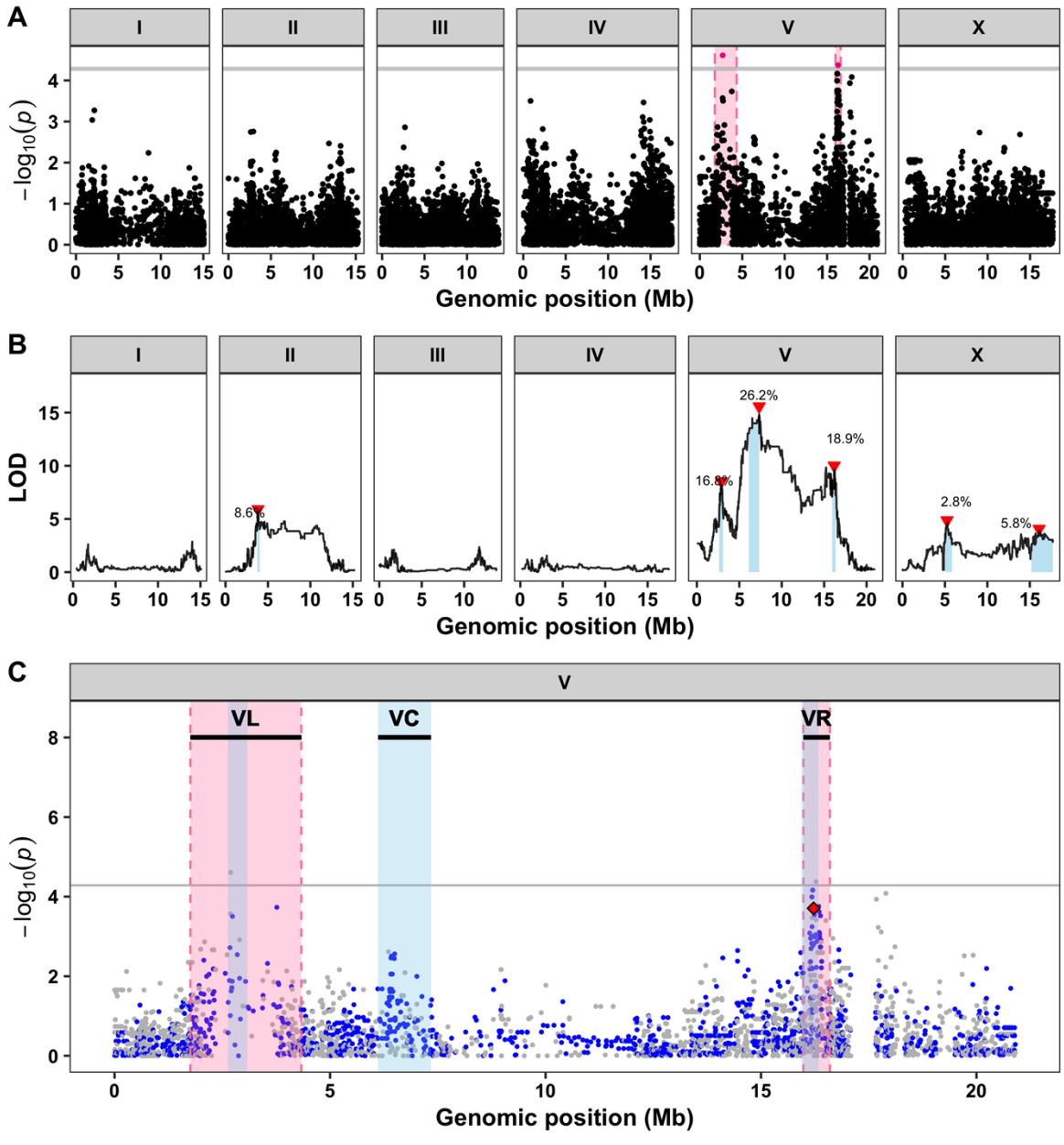

172

Fig 1. Three large-effect QTL on chromosome V control differences in abamectin responses. A) Genome-wide association mapping results for animal length (mean.TOF) are shown. Genomic position (x-axis) is plotted against the -log10(*p*) value (y-axis) for each SNV. SNVs are colored pink if they pass the genome-wide eigen-decomposition significance threshold designated by the grey line. The genomic regions of interest that pass the significance threshold are highlighted by pink rectangles. **B)** Linkage mapping results for optical density (mean.EXT) are shown. Genomic position (x-axis) is plotted against the logarithm of the odds (LOD) score (y-axis) for 13,003 genomic markers. Each significant QTL is indicated by a red triangle at the peak marker, and a blue rectangle covers the 95% confidence interval around the peak marker. The percentage of the total variance in the RIAIL population that can be explained by each QTL is shown above the QTL. **C)** Fine mapping of all common variants on chromosome V is shown. Genomic position (x-axis) is plotted against the -log10(*p*) values (y-axis) for each variant and colored by the genotype of the variant in the CB4856 strain (grey = N2 reference allele, blue = variation from the N2 reference allele). Genomic regions identified from linkage mapping analysis are highlighted in blue and genomic regions identified from association mapping are highlighted in pink. The horizontal grey line represents the genome-wide eigen-decomposition significance threshold. The red diamond represents the most significant variant in the gene *glc-1*.

Near-isogenic lines validate the independent abamectin-resistance loci on chromosome V

To empirically validate if genetic variation on chromosome V between the N2 and CB4856 strains contributes to abamectin resistance, we first generated chromosome substitution strains in which the entire chromosome V from the CB4856 strain was introgressed into the N2 genetic background or vice versa (**S8 and S9 Files**). We measured the development and reproduction of these strains and observed that the genotype on chromosome V significantly contributed to differences in abamectin resistance (**S10 File**). The strain with the CB4856 genotype on chromosome V introgressed into the N2 genetic background was significantly more resistant than the sensitive N2 strain (Tukey's HSD, *p*-value = 2.47e-06) (**S6 Fig, S10 and S11 Files**). Similarly, the strain with the N2 chromosome V introgressed into the CB4856 genetic background was significantly more sensitive to abamectin compared to the resistant CB4856 strain (Tukey's HSD, *p*-value = 0.0041, **S6 Fig, S10 and S11 Files**). These results confirm that genetic variation between the N2 and CB4856 strains at one or more

loci on chromosome V contributes to the difference in abamectin resistance between these strains.

To demonstrate that genetic variation outside the *glc-1* locus contributes to the overall resistance phenotype observed in the chromosome substitution strains, we next generated a near-isogenic line (NIL) that contains the resistant CB4856 alleles at both the VL and VC loci and the sensitive N2 allele at the VR *glc-1* locus (**Fig 2A, S8 and S9 Files**). When tested, we observed that this NIL (ECA1059) was significantly more resistant to abamectin than the sensitive N2 strain (Tukey's HSD, *p*-value = 8.83e-14) and less resistant than the resistant CB4856 strain (Tukey's HSD, *p*-value = 1.57e-13, **Fig 2B, S11 and S12 Files**). This result indicates that genetic variation on the left and/or center of chromosome V contributes to the differences in abamectin resistance between the N2 and CB4856 strains.

To further isolate the VL and VC QTL independently, we generated three NILs that each contain approximately 5 Mb of the CB4856 genome introgressed into the N2 genetic background at different locations on chromosome V so that they tile across the introgressed region in ECA1059 (**Fig 2A, S8 and S9 Files**). The strain ECA232 was not significantly more resistant to abamectin compared to the N2 strain (Tukey's HSD, *p*-value = 0.997), suggesting that this NIL has the sensitive N2 alleles at all three loci on chromosome V (**Fig 2B, S11 and S12 Files**). Alternatively, both ECA1065 and ECA377 were significantly more resistant to abamectin than the N2 strain (Tukey's HSD, *p*-values = 1.45e-13 and 5.44e-09, respectively), suggesting that the introgressed regions in both of these NILs contain one or more resistant loci (**Fig 2B, S11 and S12 Files**). Furthermore, because both strains are less resistant than the NIL with two CB4856 alleles

(ECA1059-ECA1065 *p*-value = 8.83e-14 (Tukey's HSD), ECA1059-ECA377 *p*-value = 8.83e-14 (Tukey's HSD)), we can deduce that ECA1065 and ECA377 each contain one resistant locus (**Fig 2B, S11 and S12 Files**). The introgressions in these two NILs overlap by 1.3 Mb, which leaves two possibilities: either this overlapped region (V:3,120,168-4,446,729) contains a single QTL shared by the two NILs or each NIL validates a separate QTL within the non-overlapping introgressed regions. Because we identified three QTL from linkage mapping, we believe the latter case in which ECA1065 has the CB4856 allele for the VL locus and ECA377 has the CB4856 allele for the VC locus (**Table 1, S7 Fig**).

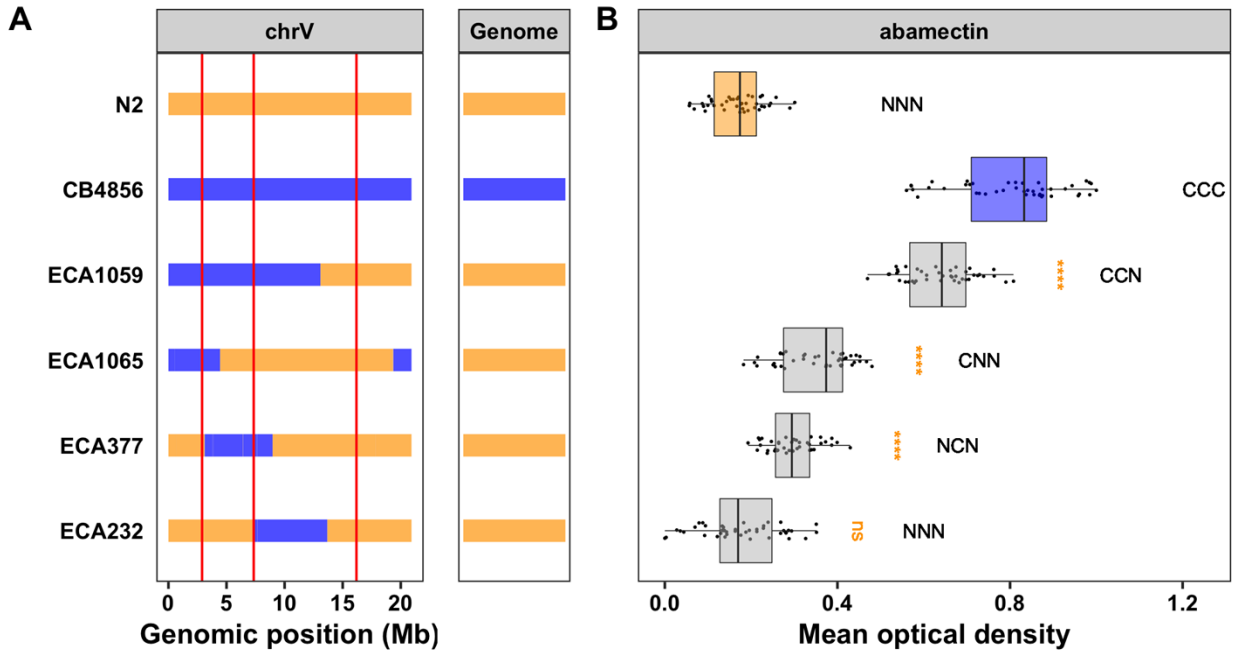

Fig 2. Near-isogenic lines confirm the additive effects of all three QTL. A) Strain genotypes are shown as colored rectangles (N2: orange, CB4856: blue) in detail for chromosome V (left box) and in general for the rest of the chromosomes (right box). The solid vertical lines represent the peak marker of each QTL. **B)** Normalized residual mean optical density in abamectin (mean.EXT, x-axis) is plotted as Tukey box plots against strain (y-axis). Statistical significance of each NIL compared to N2 calculated by Tukey's HSD is shown above each strain (ns = non-significant (p-value > 0.05), *** = significant (p-values < 0.0001). Predicted genotypes at the three QTL are shown above each strain from VL to VC to VR (N = N2 allele, C = CB4856 allele).

The VL QTL is contained within the CB4856 introgression in the NIL ECA1065 and is defined by the CB4856 introgression in the NIL ECA377 (V:1-3,120,167). This NIL-defined interval overlaps with the genomic regions identified from both linkage and association mapping (**S7 Fig, Table 1**). Using the smallest of these overlapping regions (V:2,629,324-3,076,312), we identified a total of 164 genes in the interval. A change in phenotype is most commonly driven by either genetic variation that alters the amino acid sequence of a protein (protein-coding genetic variation) or genetic variation that affects expression of one or more genes (expression variation). Using previously published gene expression data [32,34] and genetic variant data accessed from the *C. elegans* Natural Diversity Resource (CeNDR; elegansvariation.org), we eliminated 61 candidate genes because 26 genes did not harbor any genetic variation between the N2 and CB4856 strains and 35 genes had no protein-coding or expression variation. The remaining 103 candidate genes had either protein-coding or expression variation linked to this region (**S13 File**). Although none of these 103 genes encode a GluCl channel, three genes with variation in expression between the N2 and CB4856 strains do encode a cytochrome P450 (*cyp-35C1*, *cyp-33E3*, and *cyp-33E2*) and one encodes a UDP-glycosyltransferase (*ugt-53*). Previous studies have shown an upregulation of such metabolic genes in response to benzimidazole treatment [35]. Therefore, it is possible that differential expression of key metabolic genes between the N2 and CB4856 strains causes variation in abamectin resistance.

To further test the role of gene expression variation in the abamectin resistance phenotype, we measured animal development and reproduction in abamectin for 107

RIAILs for which we had existing gene expression data [32,34] (**S14 File**) and performed mediation analysis for each of the 28 genes with an eQTL in the region (**S8 Fig, S15 File**). The top three candidates from this analysis included a gene with unknown function (*F54E2.1*), an NADH Ubiquinone Oxidoreductase (*nuo-5*), and *ugt-53*. The gene *nuo-5* is a NADH-ubiquinone oxidoreductase and part of the mitochondrial complex I [36,37]. Animals deficient for *nuo-5* are more sensitive to the anthelmintic levamisole, and have defective cholinergic synaptic function [37]. Interestingly, the CB4856 strain has lower expression of both *nuo-5* and *ugt-53*, which suggests that if either of these genes are causal it is likely through an indirect mechanism. Regardless, we have previously shown that mediation analysis is a strong tool for predicting candidate genes with expression variation [32,38], and this analysis provides more evidence for the potential role of *ugt-53* or *nuo-5* in the abamectin response. However, it is important to note that this genomic interval also lies within a hyper-divergent region of the genome marked by extremely high levels of structural and single-nucleotide variation in the CB4856 strain as well as many other strains [39]. This extreme level of genetic variation could, in some cases, even cause a different composition of genes than found in the N2 reference strain. Because candidate gene predictions could be highly impacted by this divergent region, we turned our focus to the VC QTL.

The VC QTL is contained within the CB4856 introgression in the NIL ECA377 and is defined by the CB4856 introgressions in the NILs ECA1065 and ECA232 (V:4,446,729-7,374,928) (**Fig 2, S7 Fig**). This large 3 Mb interval overlaps with the genomic region identified using linkage mapping (**S7 Fig, Table 1**). We next attempted to narrow this region further by generating additional NILs with smaller introgressions (**Fig 3A, S8 and**

292 **S9 Files**) and measuring the abamectin resistance of these strains. All four NILs with the
293 CB4856 introgression on the center of chromosome V were significantly more resistant
294 (as defined by nematode length) than the N2 strain (Tukey's HSD, *p*-values < 2.83e-06,
295 **Fig 3, S11 and S16 Files**). The results for optical density were similar, but the variation
296 within strains was higher (**S9 Fig, S11 and S16 Files**). These results suggest that the
297 QTL position is contained within the smallest introgression, ECA632 (V:5,260,997-
298 5,906,132) (**Table 1, S7 Fig**). Interestingly, this NIL-defined genomic region does not
299 overlap with the confidence interval identified using linkage mapping (**Table 1, S7 Fig**).
300 Regardless, we prioritized 103 potential candidate genes with either protein-coding
301 variation and/or variation in gene expression linked to this 645 kb region (**S13 File**).
302 Notably, the glutamate-gated chloride channel, *glc-3*, resides within this narrowed region
303 (V:5,449,287, **S7 Fig**). GLC-3 was shown to be activated by ivermectin when
304 heterologously expressed in *Xenopus laevis oocytes* [40]. However, it has yet to be
305 identified in mutant screens nor directly tested for ML resistance in *C. elegans*. The
306 CB4856 strain has three rare variants in *glc-3*, including a single missense variant
307 (I439F). It is possible that one or more of these variants causes increased resistance to
308 abamectin in the CB4856 strain. In addition to *glc-3*, this list of prioritized candidate genes
309 includes one cytochrome P450 (*cyp-35B2*) and two UDP-glycosyltransferases (*ugt-51*
310 and *H23N18.4*). Mediation analysis for the 48 genes with an eQTL that maps to this region
311 highlighted several potential candidates, most noticeably *H23N18.4* (**S8 Fig, S15 File**).
312 Variation in one or more of these genes might contribute to differences in abamectin
313 resistance between the N2 and CB4856 strains.
314

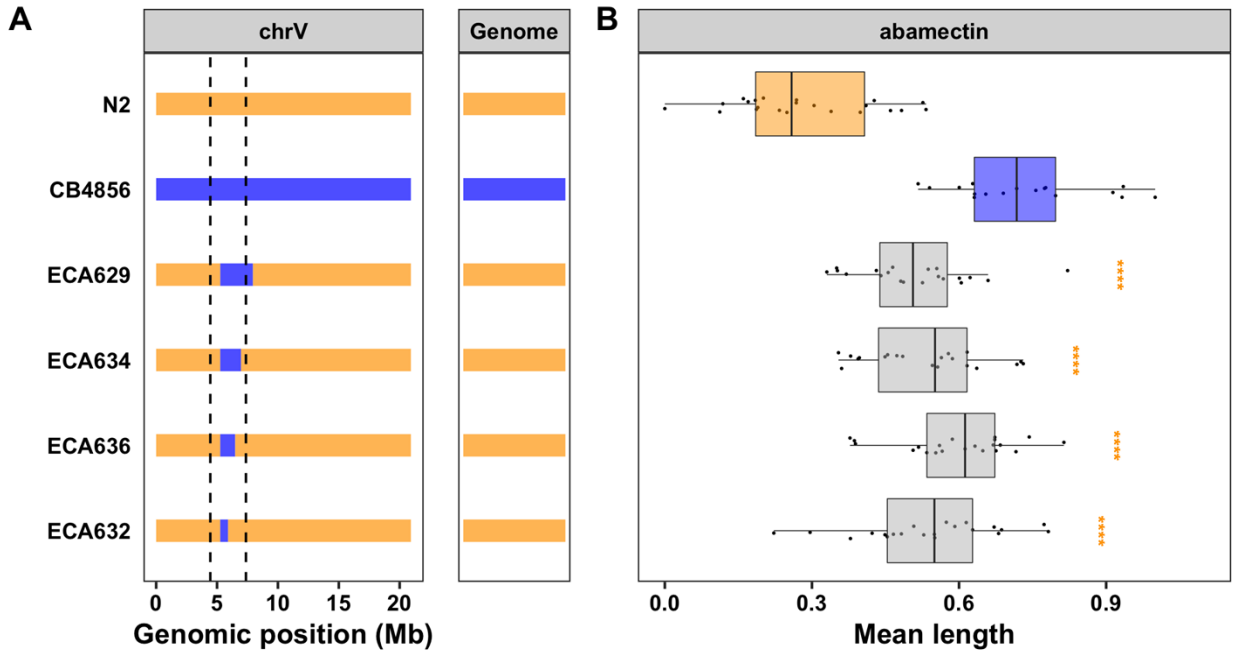

Fig 3. NILs isolate and narrow the VC QTL. A) Strain genotypes are shown as colored rectangles (N2: orange, CB4856: blue) in detail for chromosome V (left) and in general for the rest of the chromosomes (right). The dashed vertical lines represent the previous NIL-defined QTL interval for VC. **B)** Normalized residual mean animal length in abamectin (mean.TOF, x-axis) is plotted as Tukey box plots against strain (y-axis). Statistical significance of each NIL compared to N2 calculated by Tukey's HSD is shown above each strain (ns = non-significant (p-value > 0.05), *** = significant (p-values < 0.0001).

The candidate gene *lgc-54* likely does not cause macrocyclic lactone resistance

Several previous studies in parasitic nematode species have identified QTL and candidate genes that might underlie responses to ivermectin, an ML closely related to abamectin. Introgression mapping in the sheep parasite *Teladorsagia circumcincta* identified several candidate genes, including the ortholog of the *C. elegans* gene *lgc-54* [16], but this genome is highly fragmented and genomic locations are likely not correct. Regardless, this gene, similar to *glc-1*, encodes a ligand-gated chloride channel, but it has yet to be directly implicated in ML resistance. Interestingly, *lgc-54* is on the center of the *C. elegans* chromosome V (6.8 Mb) within the confidence interval for the VC QTL defined by the linkage mapping experiment but outside the NIL-defined interval (**Table 1,**

333 **S7 Fig**). Furthermore, the CB4856 strain harbors several genetic variants in this gene,
334 including a single missense variant (H42R) unique to the CB4856 strain. To test if *lgc-54*
335 plays a role in abamectin resistance in *C. elegans*, we exposed two independent *lgc-54*
336 mutants to abamectin and measured animal development and reproduction. Both *lgc-54*
337 mutants were significantly more resistant than the N2 strain (Tukey's HSD, *p*-values <
338 0.0004), which would normally provide evidence for the role of *lgc-54* in abamectin
339 resistance (**Fig 4A, S11 and S17 Files**). However, we noticed that these mutants grew
340 much slower in the control conditions than both the N2 and CB4856 strains (**Fig 4B, S17**
341 **File**). This growth defect suggests that the observed resistance is likely an artifact of the
342 statistical regression analysis, suggesting that *lgc-54* does not play a role in abamectin
343 resistance. Regardless, this system provides a strong platform for experimentally
344 validating putative resistance alleles from parasitic nematodes.
345

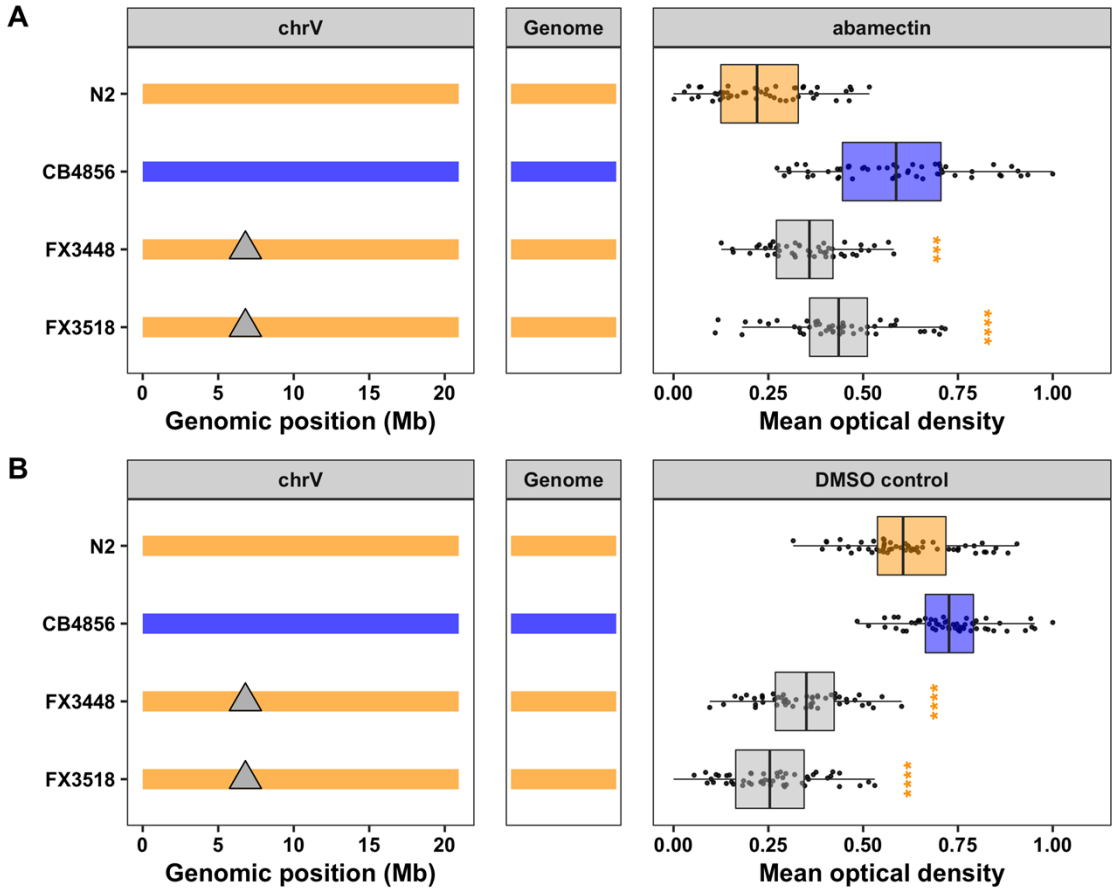

Fig 4. Testing the role of *lgc-54* in the *C. elegans* abamectin response. Strain genotypes are shown as colored rectangles (N2: orange, CB4856: blue) in detail for chromosome V (left) and in general for the rest of the chromosomes (center). Grey triangles represent mutations in the *lgc-54* gene. On the right, normalized residual mean optical density in abamectin (mean.EXT, x-axis) **(A)** or normalized mean optical density in DMSO control **(B)** is plotted as Tukey box plots against strain (y-axis). Statistical significance of each deletion strain compared to N2 calculated by Tukey's HSD is shown above each strain (ns = non-significant (p-value > 0.05), **** = significant (p-value < 0.0001).

Overlap of *C. elegans* and parasitic nematode candidate genes for macrocyclic lactone resistance

Recently, two large-effect QTL on chromosome V (37-42 Mb and 45-48 Mb) were identified in response to ivermectin treatment in *H. contortus*, a gastrointestinal parasite of small ruminants [14]. The authors found that these regions did not contain any orthologs of candidate ML resistance genes identified in *C. elegans* previously. Because the QTL for MLs in both species are found on chromosome V and the chromosomal gene

content is conserved between *C. elegans* and *H. contortus* [22], orthologs present in the QTL of both species can suggest conserved resistance mechanisms. To compare the genes in the newly defined QTL (VL and VC) to those ivermectin QTL defined for *H. contortus*, we identified one-to-one orthologs across the two species and compared chromosomal positions (**Fig 5, S18 File**). For this analysis, larger and more conservative genomic regions were selected to represent the *C. elegans* QTL (V:1-3,120,167 and V:5,260,997-7,342,129). Consistent with previous work that found that linkage groups are highly conserved but synteny (or gene order) is not [14], we found that the genes within the *C. elegans* QTL are distributed throughout the *H. contortus* chromosome V, with only 40 (21.62%) of the 185 one-to-one orthologs present in one of the two *H. contortus* QTL. Regardless, we investigated functional annotations of the one-to-one orthologs shared between the QTL and found that none have annotations that have previously been associated with ML resistance.

However, genes associated with anthelmintic resistance can be members of large gene families, like UDP-glycosyltransferases (UGTs) or cytochrome P450 enzymes (CYPs), and often do not have one-to-one orthologs. For this reason, we searched for orthogroups with more than one gene in one or both species within both QTL (**S19 File**). The complexity of comparing gene families between *C. elegans* and *H. contortus* prohibits searches for each of the 1169 genes in the VL and VC regions. Therefore, we narrowed our comparison to include one-to-many, many-to-one, and many-to-many orthologs of previously described *C. elegans* candidate genes. This approach identified orthologs for the CYP and UGT families in the *C. elegans* QTL, but none were present in the *H. contortus* QTL. Additionally, we investigated two candidate genes, *glc-3* and *nuo-5*, that

385 we identified in this study. The glutamate-gated chloride channel subunit gene, *glc-3*, is
386 located in the VC region. It has a one-to-one ortholog on *H. contortus* chromosome V, but
387 this ortholog, *HCON_00148840*, is located to the left of the *H. contortus* QTL region (27.6
388 Mb). However, the QTL location and confidence intervals depend on the underlying
389 statistics and studied populations, so this candidate gene could still play a role in *H.*
390 *contortus.* Alternatively, the one-to-one ortholog of the NADH ubiquinone oxidoreductase
391 gene, *nuo-5*, is found on the far left of *H. contortus* chromosome V (2.47 Mb) and is
392 unlikely to underlie the *H. contortus* QTL. Overall, our analysis indicates some orthologs
393 are shared between QTL or neighboring regions from the two species. These orthologs
394 should be prioritized for further studies of ML resistance.
395

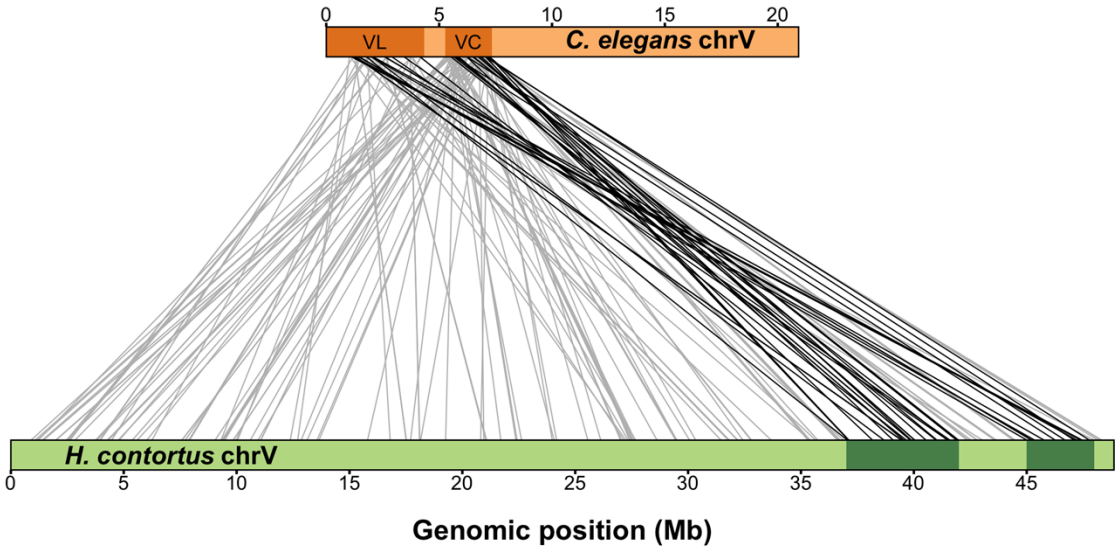

396
397

398 **Fig 5. Synteny between major-effect *C. elegans* abamectin QTL and *H. contortus* ivermectin QTL on**
399 **chromosome V.** Synteny plot showing orthologous genes between *C. elegans* (top) and *H. contortus*
400 (bottom) chromosome V. Genomic regions of interest are highlighted with dark orange (*C. elegans*) or dark
401 green (*H. contortus*) rectangles, and orthologous gene pairs are represented by connecting lines. Only
402 genes that lie within either the VL or VC *C. elegans* QTL with a one-to-one ortholog on *H. contortus*
403 chromosome V are shown (185 pairs). Grey lines represent a gene pair where the *H. contortus* ortholog is

not within a region of interest (145 pairs), and black lines represent a gene pair where the *H. contortus* ortholog is within a region of interest (40 pairs).

Discussion

In this study, we used *C. elegans* genome-wide association and linkage mapping analyses to identify three QTL on chromosome V that influence responses to the ML abamectin. One of these QTL overlaps with the previously identified GluCl gene *glc-1* [24,26]. However, the remaining two QTL are novel and might overlap with ivermectin QTL from parasitic nematodes, showing the power of using *C. elegans* to discover conserved ML resistance genes. We used NILs to validate and narrow each QTL independently. Additionally, we compared genes in our QTL with genes in two ivermectin QTL for *H. contortus* [14] and identified 40 shared orthologs. However, none of these 40 genes were strong candidates based on previous implications in ML resistance. Although we were unable to discover the specific causal genes or variants, we suggest several candidate genes within the narrowed genomic intervals that could play roles in ML resistance.

Different mapping populations and techniques detect both similar and distinct QTL

Abamectin resistance has now been mapped in *C. elegans* using three different experimental mapping techniques, five mapping populations, and several distinct traits [24,26]. Common to all these studies is the large-effect QTL detected on the right arm of chromosome V (VR locus), likely controlled by natural genetic variation in the gene *glc-1*. Here, we validated that genetic variation on the right arm of chromosome V contributes to abamectin resistance using NILs. However, further validation of the specific variants

that affect the function of *glc-1* in ML response is still needed. Regardless, the overlap of QTL between these three studies and across mapping populations suggest that the causal variant is commonly occuring and has a strong effect on ML resistance in *C. elegans* across a variety of traits.

Unlike the previous two *C. elegans* abamectin resistance mappings, we identified several additional QTL, most significantly two novel QTL on chromosome V (VL and VC). Because the previous studies that only detected *glc-1* measured swimming paralysis and survival in abamectin, it is possible that the VL and VC novel QTL could underlie differences in nematode development as measured in the high-throughput growth and fecundity assay performed here. These differences in traits and underlying QTL could suggest a complex nematode response to MLs. Although the GluCl-encoding gene, *glc-1*, underlies many of the differences across *C. elegans* strains, we show that these other loci underlie differences in development and physiology independent of *glc-1*.

The VL QTL was detected using both linkage and association mapping. The overlap of QTL from these two distinct mapping methods suggests that, like *glc-1*, genetic variation in the CB4856 strain is also found commonly across the species. Alternatively, the VC QTL was detected only with linkage mapping analysis, suggesting that either the causal variant in the CB4856 strain is rare across the species or does not cause a resistant phenotype in other wild strains. We used near-isogenic lines (NILs) to empirically validate both QTL independently. Interestingly, we show that a 645 kb region located outside of the statistically defined linkage mapping confidence interval is sufficient to cause resistance in an otherwise sensitive genetic background. Although several reasons could account for this discrepancy, it is likely that several small-effect loci on the center

of chromosome V each contribute to the overall abamectin-resistance phenotype observed in the CB4856 strain. In the recombinant population, all of these loci are jointly evaluated causing the QTL to be defined at a specific location. However, NILs are able to isolate small regions of the genome and these multiple effects can now be detected independently [38,41]. This study emphasizes that, although powerful, QTL mapping is ultimately a statistical method that can be influenced by experimental differences and that it is essential to validate QTL before drawing conclusions about the genomic location of the causal variant. Although validating QTL can be difficult in many parasitic nematode species, our ability to validate QTL in *C. elegans* is a strength of this model organism, emphasizing the need for the parasitic nematode and *C. elegans* communities to work together to push forward a cycle of discovery to understand anthelmintic modes of action and mechanisms of resistance [23].

Shared niches provide the same selective pressures for soil transmitted helminths and *C. elegans*

The potential overlap of QTL for ML resistance between *C. elegans* and parasitic nematodes suggests that the loci that confer resistance to MLs could be conserved across several nematode species. It is believed that parasitic nematodes are resistant to anthelmintic drugs because high levels of standing genetic variation harbor existing resistance alleles in a population [42,43]. Soil transmitted helminths such as *H. contortus*, spend part of their life cycle in soil or rotting vegetation, an environment that overlaps with the niche associated with the free-living *C. elegans* [44,45]. Selective pressures in this environment could originate from natural toxic compounds produced by soil-dwelling

474 bacteria and fungi from which many anthelmintic drugs are derived [46–48]. MLs, like
475 abamectin and ivermectin, are fermentation products of *Streptomyces avermitilis* [49].
476 This gram-positive bacteria was originally isolated in Japan, but shown to grow in a variety
477 of substrates [50] and its presence in the soil could select for naturally resistant
478 nematodes. Additionally, synthetic anthelmintic compounds are common soil and water
479 pollutants in some areas and can be found in runoff from farms that use anthelmintics to
480 treat agriculture or livestock [51,52]. This exposure to the same selective pressures and
481 the known genetic diversity in the *C. elegans* species suggests a method for how free-
482 living nematodes might acquire variation in the same resistance genes or gene families
483 as parasitic nematodes. In one example, it was shown that recent selective pressures
484 have likely acted on the *C. elegans ben-1* locus, causing many novel putative loss-of-
485 function alleles across the population despite evolutionary constraint on *ben-1* beta-
486 tubulin function [20]. This conclusion again highlights the relevance of using the
487 experimentally tractable *C. elegans* as a model to study anthelmintic resistance in
488 parasitic nematode species.
489
490 **Overlap of chromosome V macrocyclic lactone resistance loci between *C. elegans***
491 **and *H. contortus***
492 Genome-wide analyses in both *C. elegans* and *H. contortus* identified
493 chromosome V QTL. Because gene contents on chromosomes are highly conserved, we
494 compared these QTL intervals to look for conserved candidate genes. We initially focused
495 on one-to-one orthologs between the VL and VC QTL in *C. elegans* and both QTL in *H.*
496 *contortus* and found 40 genes but none were obvious new candidates for ML resistance.

497 This finding does not eliminate the possibility that similar responses underlie the QTL in
498 both species. The VL and VC QTL contain several gene families, including *ugt* and *cyp*
499 genes, which have been implicated in resistance previously [53,54]. Gene families often
500 evolve rapidly in response to the environment and are good candidates to confer
501 resistance [55]. Because comparisons of all gene families or ortholog groups in the VL
502 and VC QTL is difficult, we focused on ortholog groups for a subset of previously
503 described candidate gene families (*ugt* and *cyp*). Neither of these families had orthologs
504 in QTL for both species.

505 The absence of shared candidates between the QTL could be explained by the
506 statistical nature of the mapping approaches. The glutamate-gated chloride channel
507 subunit gene, *glc-3*, is located in the *C. elegans* VC QTL. Although the *H. contortus*
508 ortholog *HCON_00148840* is not located in one of the QTL, it is found on chromosome V
509 to the left of the defined QTL region (27.6 Mb) and could underlie that QTL. Alternatively,
510 *HCON_00148840* could be a candidate gene but not vary in the *H. contortus* isolates
511 used in the study [14]. Genome-wide association studies correlate genotype with
512 phenotype. These studies depend on genetic variation in the tested strains and do not
513 provide conclusive evidence on causal connections of candidate genes to resistance.
514 Further studies should use additional *H. contortus* isolates to map genomic regions that
515 correlate with ML resistance. The role of candidate genes such as *glc-3* should be tested
516 in *C. elegans*.

517 When studies in *C. elegans* and *H. contortus* do point to the same candidate
518 genes, variants that confer resistance in parasitic nematode species can be more easily
519 validated in the experimentally tractable *C. elegans* model. We showed this approach by

testing the *T. circumcincta* candidate gene (*lgc-54*) for ML resistance in *C. elegans*. Our results suggest that loss of *lgc-54* does not cause increased resistance to abamectin in *C. elegans*. A possible caveat of this study is that the decreased fitness of these mutants make the results more difficult to interpret. However, the decreased fitness could also be indicative of an essential role of *lgc-54* in nematode fitness. This study demonstrates the power of functional validation in model systems like *C. elegans* to experimentally test hypotheses for candidate genes with one-to-one orthologs. To study the resistance conferred by genes that have multiple orthologs in one or both species, genome-editing could be used to make *C. elegans* gene content resemble parasitic nematodes [23,56]. Additionally, CeNDR can be used to identify strains that have similar gene contents as found in *H. contortus* [39,57].

Power of QTL mapping in *C. elegans* to identify causal genes underlying anthelmintic resistance

This study highlights the benefits of communication between the parasite and *C. elegans* communities. Genetic mappings, screens, and selections are more easily performed in free-living nematodes and ultimately discover drug targets and mechanisms of action. However, it is important that these findings are then translated back to parasitic nematodes to confirm that genes found in *C. elegans* are responsible for drug resistance in parasites. Alternatively, candidate genes can be identified from parasitic nematode field samples and direct *C. elegans* studies to test specific genes in anthelmintic resistance traits. The potential overlap between QTL for ML resistance in *C. elegans* and *H. contortus* [14] strengthens this approach and suggests that the variants in our mapping

543 population might also confer resistance in *H. contortus* and perhaps other parasitic
544 nematode species. Future studies to discover the causal genes and variants underlying
545 our two novel QTL (VL and VC) could be informative to parasitologists and help treat
546 infected individuals more effectively.
547

548 ## Materials and Methods

549 ### Strains

550 Animals were grown on modified nematode growth media (NGMA) containing 1%
551 agar and 0.7% agarose at 20°C and fed the *E. coli* strain OP50 [58]. A total of 225
552 recombinant inbred advanced intercross lines (RIAILs) were assayed for QTL mapping
553 (set 2 RIAILs) [31]. These RIAILs were derived from a cross between QX1430, which is
554 a derivative of the canonical laboratory N2 strain that contains the CB4856 allele at the
555 *npr-1* locus and a transposon insertion in *peel-1*, and a wild isolate from Hawaii (CB4856).
556 A second set of 107 RIAILs generated previously between N2 and CB4856 [34] (set 1
557 RIAILs) were phenotyped for mediation analysis. Near-isogenic lines (NILs) were
558 generated previously by backcrossing a RIAIL of interest to either the N2 or CB4856 strain
559 for several generations using PCR amplicons covering insertion-deletion (indels) variants
560 to track the introgressed region [28]. NILs were whole-genome sequenced to verify that
561 only the targeted introgressed regions had been crossed. The *lgc-54* mutant strains
562 (FX3448 and FX3518) were obtained from the National BioResource Project (Japan). All
563 NILs and resources used to generate NILs are listed in the Supplementary Material.
564 Strains are available upon request or from the *C. elegans* Natural Diversity Resource
565 (CeNDR, elegansvariation.org) [57].

566

567 **High-throughput fitness assays**

568 A high-throughput fitness assay described previously [31] was used for all
569 phenotyping assays. In summary, each strain was passaged and amplified on NGMA
570 plates for four generations, bleach-synchronized, and 25-50 embryos were aliquoted into
571 96-well microtiter plates at a final volume of 50 µL K medium [59]. After 12 hours, arrested
572 L1s were fed HB101 bacterial lysate (Pennsylvania State University Shared Fermentation
573 Facility, State College, PA; [60]) at a final concentration of 5 mg/mL in K medium. Animals
574 were grown for 48 hours at 20°C with constant shaking. Three L4 larvae were then sorted
575 into new 96-well microtiter plates containing 10 mg/mL HB101 bacterial lysate, 50 µM
576 kanamycin, and either 1% DMSO or abamectin dissolved in 1% DMSO using a large-
577 particle flow cytometer (COPAS BIOSORT, Union Biometrica; Holliston, MA). Sorted
578 animals were grown for 96 hours at 20°C with constant shaking. The next generation of
579 animals and the parents were treated with sodium azide (50 mM in 1X M9) to straighten
580 their bodies for more accurate length measurements. Animal length (mean.TOF), optical
581 density integrated over animal length (mean.EXT), and brood size (norm.n) were
582 quantified for each well using the COPAS BIOSORT. Nematodes get longer (animal
583 length) and become thicker and more complex (optical density) over developmental time,
584 and these two traits are correlated with one another. Because these two traits are highly
585 correlated, we also generated a fourth trait (mean.norm.EXT) that normalizes the optical
586 density by length (EXT/TOF) in order to provide a means to compare optical densities
587 regardless of animal lengths.

588 Phenotypic measurements collected by the BIOSORT were processed and
589 analyzed using the R package *easysorter* [61] as described previously [28]. Differences
590 among strains within the control conditions were controlled by subtracting the mean
591 control-condition value from each drug-condition replicate for each strain using a linear
592 model (*drug_phenotype ~ mean_control_phenotype)*. In this way, we are addressing only
593 the differences among strains that were caused by the drug condition and the variance in
594 the control condition does not affect the variance in the drug condition. An R shiny web
595 app was previously developed [38] to visualize the results from the high-throughput
596 assays and can be found here: https://andersen-lab.shinyapps.io/NIL_genopheno/.
597
598 **Abamectin dose response**
599 Four genetically divergent strains (N2, CB4856, JU775, and DL238) were treated
600 with increasing concentrations of abamectin using the standard high-throughput assay
601 described above. A concentration of 5 µM abamectin (Sigma, #31732-100MG) in DMSO
602 was selected for the linkage mapping experiments and 7.5 nM abamectin in DMSO was
603 selected for the genome-wide association mapping and NIL experiments. These
604 concentrations provided a reproducible abamectin-specific effect that maximizes
605 between-strain variation and minimizes within-strain variation across the three traits. The
606 higher concentration in the linkage mapping experiment falls into the range of previously
607 reported *in vitro* assays, and the lower concentration in the GWA assay was meant to
608 capture a wider range of responses found in the natural population.
609

Genome-wide association mapping

A total of 210 wild isolates were phenotyped in both abamectin and DMSO using the standard high-throughput assay described above. A genome-wide association mapping was performed for animal optical density (mean.EXT), normalized optical density (mean.norm.EXT), length (mean.TOF), and brood size (norm.n) using the R package *cegwas2* (https://github.com/AndersenLab/cegwas2-nf) as described previously [27,33]. Genotype data were acquired from the latest VCF release (release 20200815) from CeNDR. We used BCFtools [62] to filter variants below a 5% minor allele frequency and variants with missing genotypes and used PLINK v1.9 [63,64] to prune genotypes using linkage disequilibrium. The additive kinship matrix was generated from the 21,342 markers using the *A.mat* function in the *rrBLUP* R package [65]. Because these markers have high LD, we performed eigen decomposition of the correlation matrix of the genotype matrix to identify 963 independent tests [27]. We performed genome-wide association mapping using the *GWAS* function from the *rrBLUP* package. Significance was determined by an eigenvalue threshold set by the number of independent tests in the genotype matrix [27]. Confidence intervals were defined as +/- 150 SNVs from the rightmost and leftmost markers that passed the significance threshold.

Linkage mapping

A total of 225 RIAILs [31] were phenotyped in abamectin and DMSO using the HTA described above. Linkage mapping was performed on the measured traits using the R package *linkagemapping* (https://github.com/AndersenLab/linkagemapping) as described previously [28,32]. The cross object derived from the whole-genome

633 sequencing of the RIAILs containing 13,003 SNVs was merged with the RIAIL
634 phenotypes using the *merge_pheno* function with the argument *set* = *2*. A forward search
635 (*fsearch* function) adapted from the *R/qtl* package [66] was used to calculate the logarithm
636 of the odds (LOD) scores for each genetic marker and each trait as $-n(ln(1-R^2)/2ln(10))$
637 where R is the Pearson correlation coefficient between the RIAIL genotypes at the marker
638 and trait phenotypes [67]. A 5% genome-wide error rate was calculated by permuting the
639 RIAIL phenotypes 1000 times. QTL were identified as the genetic marker with the highest
640 LOD score above the significance threshold. This marker was then integrated into the
641 model as a cofactor and mapping was repeated iteratively until no further QTL were
642 identified. Finally, the *annotate_lods* function was used to calculate the effect size of each
643 QTL and determine 95% confidence intervals defined by a 1.5 LOD drop from the peak
644 marker using the argument *cutoff* = *"proximal"*.
645
646 **Mediation analysis**
647 107 RIAILs (set 1 RIAILs) were phenotyped in both abamectin and DMSO using
648 the high-throughput assay described above. Microarray expression for 14,107 probes
649 were previously collected from the set 1 RIAILs [68], filtered [58], and mapped using
650 linkage mapping with 13,003 SNPs [32]. Mediation scores were calculated with
651 bootstrapping using *calc_mediation* function from the *linkagemapping* R package which
652 uses the *mediate* function from the *mediation* R package [69] as previously described [32]
653 for each of the probes with an eQTL within a genomic region of interest. Briefly, a mediator
654 model (expression ~ genotype) and an outcome model (phenotype ~ expression +
655 genotype) were used to calculate the proportion of the QTL effect that can be explained

by variation in gene expression. All expression and eQTL data are accessible from the *linkagemapping* R package.

Comparing macrocyclic lactone QTL between *C. elegans* and *H. contortus*

The *C. elegans* (WS273) and *H. contortus* (PRJEB506, WBPS15) [22] protein and GFF3 files were downloaded from WormBase [70] and WormBase ParaSite [71], respectively. The longest isoform of each protein-coding gene was selected using the agat_sp_keep_longest_isoform.pl script from AGAT (version 0.4.0) [72]. Filtered protein files were clustered into orthologous groups (OGs) using OrthoFinder (version 2.4.0; using the parameter *-og*) [73] and one-to-one OGs were selected. A Python script (available at https://github.com/AndersenLab/abamectin_manuscript) was used to collect the coordinates of all *C. elegans* genes within one of the identified QTL along with the coordinates of the corresponding *H. contortus* orthologs. These coordinates were used to compare synteny between the *C. elegans* abamectin QTL defined here and the *H. contortus* ivermectin QTL defined previously [14] (V: 37-42 Mb and V: 45-48 Mb).

Statistical analysis

All gene position data for the *C. elegans* genome were collected using WormBase WS273. For NIL assays, complete pairwise strain comparisons were performed on drug residual phenotypes using a *TukeyHSD* function [74] on an ANOVA model with the formula *phenotype ~ strain*. All data and scripts to generate figures can be found at https://github.com/AndersenLab/abamectin_manuscript.

Acknowledgements

We would like to thank members of the Andersen laboratory for their helpful comments on the manuscript. We would also like to thank WormBase for hosting both parasite and *C. elegans* genomes and annotations and the *C. elegans* Natural Diversity Resource (NSF CSBR 1930382) for data and tools critical for our analysis. We would also like to thank the National BioResource Project (Japan) for the *lgc-54* mutant strains (FX3448 and FX3518).

References

1. Hotez PJ, Alvarado M, Basáñez M-G, Bolliger I, Bourne R, Boussinesq M, et al. The global burden of disease study 2010: interpretation and implications for the neglected tropical diseases. PLoS Negl Trop Dis. 2014;8: e2865. doi:10.1371/journal.pntd.0002865

2. Kahn LP, Woodgate RG. Integrated parasite management: products for adoption by the Australian sheep industry. Vet Parasitol. 2012;186: 58–64. doi:10.1016/j.vetpar.2011.11.046

3. Sutherland IA, Leathwick DM. Anthelmintic resistance in nematode parasites of cattle: a global issue? Trends Parasitol. 2011;27: 176–181. doi:10.1016/j.pt.2010.11.008

4. Hotez PJ, Fenwick A, Savioli L, Molyneux DH. Rescuing the bottom billion through control of neglected tropical diseases. Lancet. 2009;373: 1570–1575. doi:10.1016/S0140-6736(09)60233-6

5. Lustigman S, Prichard RK, Gazzinelli A, Grant WN, Boatin BA, McCarthy JS, et al. A research agenda for helminth diseases of humans: the problem of helminthiases. PLoS Negl Trop Dis. 2012;6: e1582. doi:10.1371/journal.pntd.0001582

6. Charlier J, van der Voort M, Kenyon F, Skuce P, Vercruysse J. Chasing helminths and their economic impact on farmed ruminants. Trends Parasitol. 2014;30: 361–367. doi:10.1016/j.pt.2014.04.009

7. Kotze AC, Prichard RK. Anthelmintic Resistance in Haemonchus contortus: History, Mechanisms and Diagnosis. Adv Parasitol. 2016;93: 397–428. doi:10.1016/bs.apar.2016.02.012

8. Ásbjörnsdóttir KH, Means AR, Werkman M, Walson JL. Prospects for elimination of soil-transmitted helminths. Current Opinion in Infectious Diseases. 2017. pp. 482–488. doi:10.1097/qco.0000000000000395

9. Orr AR, Quagraine JE, Suwondo P, George S, Harrison LM, Dornas FP, et al. Genetic Markers of Benzimidazole Resistance among Human Hookworms (Necator americanus) in Kintampo North Municipality, Ghana. Am J Trop Med Hyg. 2019;100: 351–356. doi:10.4269/ajtmh.18-0727

10. Wolstenholme AJ, Fairweather I, Prichard R, von Samson-Himmelstjerna G, Sangster NC. Drug resistance in veterinary helminths. Trends Parasitol. 2004;20: 469–476. doi:10.1016/j.pt.2004.07.010

11. McCavera S, Walsh TK, Wolstenholme AJ. Nematode ligand-gated chloride channels: an appraisal of their involvement in macrocyclic lactone resistance and prospects for developing molecular markers. Parasitology. 2007;134: 1111–1121.

722 doi:10.1017/S0031182007000042

723 12. Dent JA, Smith MM, Vassilatis DK, Avery L. The genetics of ivermectin resistance
724 in Caenorhabditis elegans. Proc Natl Acad Sci U S A. 2000;97: 2674–2679.
725 doi:10.1073/pnas.97.6.2674

726 13. Page AP. The sensory amphidial structures of Caenorhabditis elegans are involved
727 in macrocyclic lactone uptake and anthelmintic resistance. Int J Parasitol. 2018;48:
728 1035–1042. doi:10.1016/j.ijpara.2018.06.003

729 14. Doyle SR, Illingworth CJR, Laing R, Bartley DJ, Redman E, Martinelli A, et al.
730 Population genomic and evolutionary modelling analyses reveal a single major QTL
731 for ivermectin drug resistance in the pathogenic nematode, Haemonchus contortus.
732 BMC Genomics. 2019;20: 218. doi:10.1186/s12864-019-5592-6

733 15. Rezansoff AM, Laing R, Gilleard JS. Evidence from two independent backcross
734 experiments supports genetic linkage of microsatellite Hcms8a20, but not other
735 candidate loci, to a major ivermectin resistance locus in Haemonchus contortus.
736 International Journal for Parasitology. 2016. pp. 653–661.
737 doi:10.1016/j.ijpara.2016.04.007

738 16. Choi Y-J, Bisset SA, Doyle SR, Hallsworth-Pepin K, Martin J, Grant WN, et al.
739 Genomic introgression mapping of field-derived multiple-anthelmintic resistance in
740 Teladorsagia circumcincta. PLoS Genet. 2017;13: e1006857.
741 doi:10.1371/journal.pgen.1006857

742 17. Stear MJ, Boag B, Cattadori I, Murphy L. Genetic variation in resistance to mixed,
743 predominantly Teladorsagia circumcincta nematode infections of sheep: from
744 heritabilities to gene identification. Parasite Immunol. 2009;31: 274–282.
745 doi:10.1111/j.1365-3024.2009.01105.x

746 18. Doyle SR, Bourguinat C, Nana-Djeunga HC, Kengne-Ouafo JA, Pion SDS, Bopda
747 J, et al. Genome-wide analysis of ivermectin response by Onchocerca volvulus
748 reveals that genetic drift and soft selective sweeps contribute to loss of drug
749 sensitivity. PLoS Negl Trop Dis. 2017;11: e0005816.
750 doi:10.1371/journal.pntd.0005816

751 19. Zamanian M, Cook DE, Zdraljevic S, Brady SC, Lee D, Lee J, et al. Discovery of
752 genomic intervals that underlie nematode responses to benzimidazoles. PLoS Negl
753 Trop Dis. 2018;12: e0006368. doi:10.1371/journal.pntd.0006368

754 20. Hahnel SR, Zdraljevic S, Rodriguez BC, Zhao Y, McGrath PT, Andersen EC.
755 Extreme allelic heterogeneity at a Caenorhabditis elegans beta-tubulin locus
756 explains natural resistance to benzimidazoles. PLoS Pathog. 2018;14: e1007226.
757 doi:10.1371/journal.ppat.1007226

758 21. Gilleard JS. Haemonchus contortus as a paradigm and model to study anthelmintic
759 drug resistance. Parasitology. 2013;140: 1506–1522.

doi:10.1017/S0031182013001145

22. Doyle SR, Tracey A, Laing R, Holroyd N, Bartley D, Bazant W, et al. Genomic and transcriptomic variation defines the chromosome-scale assembly of Haemonchus contortus, a model gastrointestinal worm. Commun Biol. 2020;3: 656. doi:10.1038/s42003-020-01377-3

23. Wit J, Dilks CM, Andersen EC. Complementary Approaches with Free-living and Parasitic Nematodes to Understanding Anthelmintic Resistance. Trends Parasitol. 2020. doi:10.1016/j.pt.2020.11.008

24. Ghosh R, Andersen EC, Shapiro JA, Gerke JP, Kruglyak L. Natural variation in a chloride channel subunit confers avermectin resistance in C. elegans. Science. 2012;335: 574–578. doi:10.1126/science.1214318

25. Dilks CM, Hahnel SR, Sheng Q, Long L, McGrath PT, Andersen EC. Quantitative benzimidazole resistance and fitness effects of parasitic nematode beta-tubulin alleles. bioRxiv. 2020. p. 2020.07.07.191866. doi:10.1101/2020.07.07.191866

26. Burga A, Ben-David E, Lemus Vergara T, Boocock J, Kruglyak L. Fast genetic mapping of complex traits in C. elegans using millions of individuals in bulk. Nat Commun. 2019;10: 2680. doi:10.1038/s41467-019-10636-9

27. Zdraljevic S, Fox BW, Strand C, Panda O, Tenjo FJ, Brady SC, et al. Natural variation in C. elegans arsenic toxicity is explained by differences in branched chain amino acid metabolism. Elife. 2019;8. doi:10.7554/eLife.40260

28. Brady SC, Zdraljevic S, Bisaga KW, Tanny RE, Cook DE, Lee D, et al. A Novel Gene Underlies Bleomycin-Response Variation in Caenorhabditis elegans. Genetics. 2019;212: 1453–1468. doi:10.1534/genetics.119.302286

29. Evans KS, Brady SC, Bloom JS, Tanny RE, Cook DE, Giuliani SE, et al. Shared Genomic Regions Underlie Natural Variation in Diverse Toxin Responses. Genetics. 2018. doi:10.1534/genetics.118.301311

30. Zdraljevic S, Strand C, Seidel HS, Cook DE, Doench JG, Andersen EC. Natural variation in a single amino acid substitution underlies physiological responses to topoisomerase II poisons. PLoS Genet. 2017;13: e1006891. doi:10.1371/journal.pgen.1006891

31. Andersen EC, Shimko TC, Crissman JR, Ghosh R, Bloom JS, Seidel HS, et al. A Powerful New Quantitative Genetics Platform, Combining Caenorhabditis elegans High-Throughput Fitness Assays with a Large Collection of Recombinant Strains. G3 . 2015;5: 911–920. doi:10.1534/g3.115.017178

32. Evans KS, Andersen EC. The Gene scb-1 Underlies Variation in Caenorhabditis elegans Chemotherapeutic Responses. G3 . 2020. doi:10.1534/g3.120.401310

33. Evans KS, Zdraljevic S, Stevens L, Collins K, Tanny RE, Andersen EC. Natural variation in the sequestosome-related gene, sqst-5, underlies zinc homeostasis in Caenorhabditis elegans. bioRxiv. 2020. p. 2020.07.10.196857. doi:10.1101/2020.07.10.196857

34. Rockman MV, Kruglyak L. Recombinational landscape and population genomics of Caenorhabditis elegans. PLoS Genet. 2009;5: e1000419. doi:10.1371/journal.pgen.1000419

35. Stasiuk SJ, MacNevin G, Workentine ML, Gray D, Redman E, Bartley D, et al. Similarities and differences in the biotransformation and transcriptomic responses of Caenorhabditis elegans and Haemonchus contortus to five different benzimidazole drugs. Int J Parasitol Drugs Drug Resist. 2019;11: 13–29. doi:10.1016/j.ijpddr.2019.09.001

36. Hansen M, Hsu A-L, Dillin A, Kenyon C. New genes tied to endocrine, metabolic, and dietary regulation of lifespan from a Caenorhabditis elegans genomic RNAi screen. PLoS Genet. 2005;1: 119–128. doi:10.1371/journal.pgen.0010017

37. Maglioni S, Schiavi A, Melcher M, Brinkmann V, Luo Z, Raimundo N, et al. Lutein restores synaptic functionality in a C. elegans model for mitochondrial complex I deficiency. doi:10.1101/2020.02.20.957225

38. Evans KS, Zdraljevic S, Stevens L, Collins K, Tanny RE, Andersen EC. Natural variation in the sequestosome-related gene, sqst-5, underlies zinc homeostasis in Caenorhabditis elegans. PLoS Genet. 2020;16: e1008986. doi:10.1371/journal.pgen.1008986

39. Lee D, Zdraljevic S, Stevens L, Wang Y, Tanny RE, Crombie TA, et al. Balancing selection maintains ancient genetic diversity in C. elegans. 2020. p. 2020.07.23.218420. doi:10.1101/2020.07.23.218420

40. Horoszok L, Raymond V, Sattelle DB, Wolstenholme AJ. GLC-3: a novel fipronil and BIDN-sensitive, but picrotoxinin-insensitive, L-glutamate-gated chloride channel subunit from Caenorhabditis elegans. Br J Pharmacol. 2001;132: 1247–1254. doi:10.1038/sj.bjp.0703937

41. Bernstein MR, Zdraljevic S, Andersen EC, Rockman MV. Tightly linked antagonistic-effect loci underlie polygenic phenotypic variation in C. elegans. Evol Lett. 2019;3: 462–473. doi:10.1002/evl3.139

42. Redman E, Whitelaw F, Tait A, Burgess C, Bartley Y, Skuce PJ, et al. The emergence of resistance to the benzimidazole anthlemintics in parasitic nematodes of livestock is characterised by multiple independent hard and soft selective sweeps. PLoS Negl Trop Dis. 2015;9: e0003494. doi:10.1371/journal.pntd.0003494

43. Gilleard JS, Redman E. Chapter Two - Genetic Diversity and Population Structure of Haemonchus contortus. In: Gasser RB, Samson-Himmelstjerna GV, editors.

834 Advances in Parasitology. Academic Press; 2016. pp. 31–68.
835 doi:10.1016/bs.apar.2016.02.009

836 44. Frézal L, Félix M-A. C. elegans outside the Petri dish. Elife. 2015;4.
837 doi:10.7554/eLife.05849

838 45. Crombie TA, Zdraljevic S, Cook DE, Tanny RE, Brady SC, Wang Y, et al. Deep
839 sampling of Hawaiian Caenorhabditis elegans reveals high genetic diversity and
840 admixture with global populations. Elife. 2019;8: e50465. doi:10.7554/eLife.50465

841 46. Campbell WC. History of avermectin and ivermectin, with notes on the history of
842 other macrocyclic lactone antiparasitic agents. Curr Pharm Biotechnol. 2012;13:
843 853–865. doi:10.2174/138920112800399095

844 47. Campbell WC. Serendipity and new drugs for infectious disease. ILAR J. 2005;46:
845 352–356. doi:10.1093/ilar.46.4.352

846 48. Alivisatos SG, Lamantia L, Matijevitch BL. Imidazolytic processes. VI. Enzymic
847 formation of benzimidazole and 5,6-dimethylbenzimidazole containing
848 dinucleotides. Biochim Biophys Acta. 1962;58: 209–217. doi:10.1016/0006-
849 3002(62)91000-4

850 49. Õmura S, Crump A. The life and times of ivermectin — a success story. Nature
851 Reviews Microbiology. 2004. pp. 984–989. doi:10.1038/nrmicro1048

852 50. Burg RW, Miller BM, Baker EE, Birnbaum J, Currie SA, Hartman R, et al.
853 Avermectins, new family of potent anthelmintic agents: producing organism and
854 fermentation. Antimicrob Agents Chemother. 1979;15: 361–367.
855 doi:10.1128/aac.15.3.361

856 51. Cycoń M, Mrozik A, Piotrowska-Seget Z. Bioaugmentation as a strategy for the
857 remediation of pesticide-polluted soil: A review. Chemosphere. 2017;172: 52–71.
858 doi:10.1016/j.chemosphere.2016.12.129

859 52. Taube J, Vorkamp K, Förster M, Herrmann R. Pesticide residues in biological
860 waste. Chemosphere. 2002;49: 1357–1365. doi:10.1016/s0045-6535(02)00503-9

861 53. Whittaker JH, Carlson SA, Jones DE, Brewer MT. Molecular mechanisms for
862 anthelmintic resistance in strongyle nematode parasites of veterinary importance. J
863 Vet Pharmacol Ther. 2017;40: 105–115. doi:10.1111/jvp.12330

864 54. Matoušková P, Vokřál I, Lamka J, Skálová L. The Role of Xenobiotic-Metabolizing
865 Enzymes in Anthelmintic Deactivation and Resistance in Helminths. Trends
866 Parasitol. 2016;32: 481–491. doi:10.1016/j.pt.2016.02.004

867 55. Curran DM, Gilleard JS, Wasmuth JD. MIPhy: identify and quantify rapidly evolving
868 members of large gene families. PeerJ. 2018;6: e4873. doi:10.7717/peerj.4873

869 56. Zamanian M, Andersen EC. Prospects and challenges of CRISPR/Cas genome
870 editing for the study and control of neglected vector-borne nematode diseases. The
871 FEBS Journal. 2016. pp. 3204–3221. doi:10.1111/febs.13781

872 57. Cook DE, Zdraljevic S, Roberts JP, Andersen EC. CeNDR, the Caenorhabditis
873 elegans natural diversity resource. Nucleic Acids Res. 2016.
874 doi:10.1093/nar/gkw893

875 58. Andersen EC, Bloom JS, Gerke JP, Kruglyak L. A variant in the neuropeptide
876 receptor npr-1 is a major determinant of Caenorhabditis elegans growth and
877 physiology. PLoS Genet. 2014;10: e1004156. doi:10.1371/journal.pgen.1004156

878 59. Boyd WA, Smith MV, Freedman JH. Caenorhabditis elegans as a model in
879 developmental toxicology. Methods Mol Biol. 2012;889: 15–24. doi:10.1007/978-1-
880 61779-867-2_3

881 60. García-González AP, Ritter AD, Shrestha S, Andersen EC, Yilmaz LS, Walhout
882 AJM. Bacterial Metabolism Affects the C. elegans Response to Cancer
883 Chemotherapeutics. Cell. 2017;169: 431–441.e8. doi:10.1016/j.cell.2017.03.046

884 61. Shimko TC, Andersen EC. COPASutils: an R package for reading, processing, and
885 visualizing data from COPAS large-particle flow cytometers. PLoS One. 2014;9:
886 e111090. doi:10.1371/journal.pone.0111090

887 62. Li H. A statistical framework for SNP calling, mutation discovery, association
888 mapping and population genetical parameter estimation from sequencing data.
889 Bioinformatics. 2011;27: 2987–2993. doi:10.1093/bioinformatics/btr509

890 63. Purcell S, Neale B, Todd-Brown K, Thomas L, Ferreira MAR, Bender D, et al.
891 PLINK: a tool set for whole-genome association and population-based linkage
892 analyses. Am J Hum Genet. 2007;81: 559–575. doi:10.1086/519795

893 64. Chang CC, Chow CC, Tellier LC, Vattikuti S, Purcell SM, Lee JJ. Second-
894 generation PLINK: rising to the challenge of larger and richer datasets.
895 Gigascience. 2015;4: 7. doi:10.1186/s13742-015-0047-8

896 65. Endelman JB. Ridge Regression and Other Kernels for Genomic Selection with R
897 Package rrBLUP. Plant Genome. 2011;4: 250–255.
898 doi:10.3835/plantgenome2011.08.0024

899 66. Broman KW, Wu H, Sen S, Churchill GA. R/qtl: QTL mapping in experimental
900 crosses. Bioinformatics. 2003;19: 889–890. Available:
901 https://www.ncbi.nlm.nih.gov/pubmed/12724300

902 67. Bloom JS, Ehrenreich IM, Loo WT, Lite T-LV, Kruglyak L. Finding the sources of
903 missing heritability in a yeast cross. Nature. 2013;494: 234–237.
904 doi:10.1038/nature11867

68. Rockman MV, Skrovanek SS, Kruglyak L. Selection at linked sites shapes heritable phenotypic variation in C. elegans. Science. 2010;330: 372–376. doi:10.1126/science.1194208

69. Tingley D, Yamamoto T, Hirose K, Keele L, Imai K. mediation: R Package for Causal Mediation Analysis. Journal of Statistical Software, Articles. 2014;59: 1–38. doi:10.18637/jss.v059.i05

70. Harris TW, Arnaboldi V, Cain S, Chan J, Chen WJ, Cho J, et al. WormBase: a modern Model Organism Information Resource. Nucleic Acids Res. 2020;48: D762–D767. doi:10.1093/nar/gkz920

71. Howe KL, Bolt BJ, Shafie M, Kersey P, Berriman M. WormBase ParaSite - a comprehensive resource for helminth genomics. Mol Biochem Parasitol. 2017;215: 2–10. doi:10.1016/j.molbiopara.2016.11.005

72. Dainat J, Hereñú D, Pucholt P. NBISweden/AGAT: AGAT-v0.5.1. 2020. doi:10.5281/zenodo.4205393

73. Emms DM, Kelly S. OrthoFinder: phylogenetic orthology inference for comparative genomics. Genome Biol. 2019;20: 238. doi:10.1186/s13059-019-1832-y

74. R Core Team. R: A Language and Environment for Statistical Computing. Vienna, Austria: R Foundation for Statistical Computing; 2017. Available: https://www.R-project.org/

Supporting information captions

S1 Fig. Dose response with four divergent wild isolates. Results from the abamectin dose response HTA for brood size (norm.n), animal length (mean.TOF), animal optical density (mean.EXT), and normalized optical density (mean.norm.EXT) are shown. For each trait, drug concentration (nM) (x-axis) is plotted against phenotype subtracted from control (y-axis) and colored by strain (CB4856: blue, DL238: green, JU775: purple, N2: orange). A concentration of 7.5 nM was chosen for future experiments.

S2 Fig. Genome-wide association mappings identify six QTL across three traits in response to abamectin. A) Normalized residual phenotype (y-axis) of 210 wild isolates (x-axis) in response to abamectin. **B)** Association mapping results are shown. Genomic position (x-axis) is plotted against the -log10*(p)* value (y-axis) for each SNV. SNVs are colored pink if they pass the genome-wide eigen-decomposition significance threshold designated by the grey line. The genomic regions of interest that pass the significance threshold are highlighted by pink rectangles. **C)** For each QTL, the normalized residual phenotype (y-axis) of strains split by genotype at the peak marker (x-axis) are plotted as Tukey box plots. Each point corresponds to a wild isolate strain. Strains with the N2 reference allele are colored grey, and strains with an alternative allele are colored pink.

S3 Fig. Linkage mapping identifies 14 QTL across four traits in response to abamectin. A) Normalized residual phenotype (y-axis) of 225 RIAILs (x-axis) in response to abamectin. The parental strains are colored: N2, orange; CB4856, blue. **B)** Linkage mapping results are shown. Genomic position in Mb (x-axis) is plotted against the logarithm of the odds (LOD) score (y-axis) for 13,003 genomic markers. Each significant QTL is indicated by a red triangle at the peak marker, and a blue rectangle shows the

948 95% confidence interval around the peak marker. The percentage of the total variance in
949 the RIAIL population that can be explained by each QTL is shown above the QTL. **C)** For
950 each QTL, the normalized residual phenotype (y-axis) of RIAILs split by genotype at the
951 marker with the maximum LOD score (x-axis) are plotted as Tukey box plots. Each point
952 corresponds to a unique recombinant strain. Strains with the N2 allele are colored orange,
953 and strains with the CB4856 allele are colored blue.

954 **S4 Fig. Summary of QTL mapping for responses to abamectin.** Genomic positions
955 (x-axis) of all QTL identified from linkage mapping (top) and association mapping (bottom)
956 are shown for each drug-trait (y-axis). Each QTL is plotted as a point at the genomic
957 location of the peak marker and a line that represents the confidence interval. QTL are
958 colored by the significance of the LOD score (linkage) or -log10(*p*) value (association),
959 increasing from purple to green to yellow.

960 **S5 Fig. Two-dimensional genome scan for mean optical density (mean.EXT) in**
961 **abamectin.** Log of the odds (LOD) scores are shown for each pairwise combination of
962 loci, split by chromosome. The upper-left triangle contains the epistasis LOD scores
963 (interaction effects), and the lower-right triangle contains the LOD scores for the full model
964 (both interaction and additive effects). LOD scores are colored by significance, increasing
965 from purple to green to yellow. The LOD scores for the epistasis model are shown on the
966 left of the color scale, and the LOD scores for the full model are shown on the right.

967 **S6 Fig. Chromosome substitution strains validate the existence of one or more**
968 **resistance loci on chromosome V. A)** Strain genotypes are shown as colored
969 rectangles (N2: orange, CB4856: blue) in detail for chromosome V (left) and in general
970 for the rest of the chromosomes (right). **B)** Normalized residual mean lengths in

971 abamectin (mean.TOF, x-axis) are plotted as Tukey box plots against strain (y-axis).
972 Statistical significance of each NIL as compared to its parental strain (ECA573 to N2 and
973 ECA554 to CB4856) calculated by Tukey's HSD is shown above each strain (ns = non-
974 significant (p-value > 0.05); *, **, ***, and *** = significant (p-value < 0.05, 0.01, 0.001, or
975 0.0001, respectively).

976 **S7 Fig. Refining QTL positions with NILs. A)** Fine mapping of all common variants on
977 chromosome V is shown. Genomic position (x-axis) is plotted against the -log10(*p*) values
978 (y-axis) for each variant and colored by the genotype of the variant in the CB4856 strain
979 (grey = N2 reference allele, blue = variation from the N2 reference allele). Genomic
980 regions identified from linkage mapping analysis are highlighted in blue and genomic
981 regions identified from association mapping are highlighted in pink. The horizontal grey
982 line represents the genome-wide eigen-decomposition significance threshold. The red
983 points represent the positions of the most significant variants in the genes *glc-1*
984 (diamond), *glc-3* (circle), and *lgc-54* (square). The vertical lines represent the smallest
985 NIL-defined genomic region for the VL (solid), VC (dashed), and VR (dotted) QTL. **B)**
986 Strain genotypes are shown as colored rectangles (N2: orange, CB4856: blue) in detail
987 for chromosome V. The vertical lines represent the smallest NIL-defined genomic region
988 for the VL (solid), VC (dashed), and VR (dotted) QTL.

989 **S8 Fig. Mediation analysis for the VL and VC QTL.** Mediation estimates calculated as
990 the indirect effect that differences in expression of each gene plays in the overall
991 phenotype (y-axis) are plotted against genomic position of the eQTL (x-axis) on
992 chromosome V for all genes with a gene expression QTL in the narrowed VL and VC
993 intervals. The 90th percentile of the distribution of mediation estimates is represented by

994 the horizontal grey line. The confidence of the estimate increases (*p*-value decreases) as
995 points become more solid.

996 **S9 Fig. NILs validate and narrow the VC QTL. A)** Strain genotypes are shown as
997 colored rectangles (N2: orange, CB4856: blue) in detail for chromosome V (left) and in
998 general for the rest of the chromosomes (right). The dashed vertical lines represent the
999 previous NIL-defined QTL interval for VC. **B)** Normalized residual mean optical densities
1000 in abamectin (mean.EXT, x-axis) are plotted as Tukey box plots against strain (y-axis).
1001 Statistical significance of each NIL as compared to the N2 strain calculated by Tukey's
1002 HSD is shown above each strain (ns = non-significant (p-value > 0.05); *, **, ***, and ***
1003 = significant (p-value < 0.05, 0.01, 0.001, or 0.0001, respectively).

1004 **S1 File. Dose response phenotype data.** Results of the dose response for the genome-
1005 wide association high-throughput fitness assay

1006 **S2 File. Wild isolate phenotype data.** Residual phenotypic values for the 210 wild
1007 isolates in response to abamectin

1008 **S3 File. Association mapping results.** Genome-wide association mapping results for
1009 all four drug-response traits tested in the high-throughput fitness assay

1010 **S4 File. RIAIL phenotype data.** Residual phenotypic values for the 225 set 2 RIAILs in
1011 response to abamectin

1012 **S5 File. Linkage mapping results.** Linkage mapping LOD scores at 13,003 genomic
1013 markers for all four drug-response traits with the set 2 RIAILs

1014 **S6 File. Summary of two-dimensional genome scan.** Summary of the scan2 object
1015 containing data from the two-dimensional genome scan with animal optical density
1016 (mean.EXT) in abamectin

S7 File. Chromosome V variants. Correlation values and annotations for all variants on chromosome V

S8 File. NIL sequence data. VCF from the whole-genome sequencing for all the NILs in this study

S9 File. NIL genotype data. Simplified genotypes of the NILs in the study

S10 File. CSSV phenotype data. Raw pruned phenotypes for the high-throughput fitness assay with the chromosome V substitution strains

S11 File. Statistical significance for NIL assays. Pairwise statistical significance for all strains and high-throughput assays

S12 File. ChrV NIL breakup phenotype data. Raw pruned phenotypes for the NILs used to break up the QTL interval on chromosome V

S13 File. Candidate genes on chrV. List of all genes in the chromosome VL and VC intervals, their functional descriptions and GO annotations, and if they have variation in CB4856

S14 File. Set 1 RIAIL phenotype data. Residual phenotypic values for the 107 set 1 RIAILs in response to abamectin

S15 File. Mediation estimates for chrV QTL. Mediation estimates for the chromosome VL and VC QTL

S16 File. NILs to narrow VC QTL. Raw pruned phenotypes for the chromosome VC NIL high-throughput fitness assay

S17 File. lgc-54 mutant phenotypes. Raw pruned phenotypes for the the lgc-54 deletion strains high-throughput fitness assay

1039 **S18 File. One-to-one orthologous genes in *H. contortus*.** Coordinates and orthologous

1040 relationships for *H. contortus* QTL

1041 **S19 File. Orthogroups for *H. contortus* and *C. elegans* genes.** Contains a list of all

1042 the genes found in each orthogroup between *C. elegans* and *H. contortus*